Numerical modeling of multiphase first-contact miscible flows. Part 1. Analytical Riemann solver

Ruben Juanes[1] and Knut–Andreas Lie[2]

[1] Stanford University, Department of Petroleum Engineering
65 Green Earth Sciences Building, Stanford, CA 94305, USA

[2] SINTEF ICT, Department of Applied Mathematics
P.O. Box 124 Blindern, NO-0314 Oslo, Norway

Submitted to *Transport in Porous Media*

October 24, 2005

Abstract

In this series of two papers we present a front-tracking method for the numerical simulation of first-contact miscible gas injection processes. The method is developed for constructing very accurate (or even exact) solutions to one-dimensional initial-boundary-value problems in the form of a set of evolving discontinuities. The evolution of the discontinuities is given by analytical solutions to Riemann problems. In this paper, we present the mathematical model of the problem and the complete Riemann solver, that is, the analytical solution to the one-dimensional problem with piecewise constant initial data separated by a single discontinuity, for any left and right states. The Riemann solver presented here is the building block for the front-tracking/streamline method described and applied in the second paper.

KEY WORDS: porous media, miscible displacement, first-contact miscible, shocks, Riemann problem, analytical solution

1 Introduction

Gas injection is one of the most widely used enhanced oil recovery processes [1–3]. The fundamental principle is the development of miscibility between the resident oil phase and the injected gas, in order to enhance the mobility of the hydrocarbon phase and to achieve a high displacement efficiency. In general, miscibility between the oil present in the reservoir and the injected

gas leads to a complex set of interactions described by thermodynamical equilibrium of the system, in which components of the gas dissolve in the oil, and components of the oil transfer to the vapor [4–6].

In this series of two papers, we restrict our attention to simplified thermodynamical systems that can be approximated by *first-contact miscible* phase behavior. The underlying assumption is that the injection gas (solvent) and the resident oil mix in all proportions to form a single hydrocarbon phase. This scenario is optimal with respect to local displacement efficiency, and can be achieved in practice if the gas is injected at a pressure well above the minimum miscibility pressure [7; 8].

We present a computational framework for the efficient simulation of first-contact miscible processes in three-dimensional, heterogeneous reservoir models. The key ingredients of our approach are:

1. An analytical solution of the one-dimensional Riemann problem for a three-component, two-phase system under the assumption of first-contact miscibility of the hydrocarbon components, assuming that the effects of viscous fingering are negligible.

2. A front-tracking algorithm that makes use of the analytical Riemann solver as a building block for obtaining approximate solutions to general one-dimensional problems.

3. A streamline simulator that decouples the three-dimensional transport equations into a set of one-dimensional problems along streamlines.

In Part 1, we present the mathematical model of the problem and the complete set of analytical solutions to the Riemann problem. In Part 2, we describe the front-tracking algorithm and streamline simulation framework, along with representative numerical examples in one-, two- and three-dimensional problems.

The proposed framework was employed by the authors for the simulation of immiscible three-phase flow [9; 10], and it is extended here to miscible gas injection problems. The applicability of the framework presented here is limited, however, by the assumption that the effects of viscous fingering are not accounted for. New analytical solutions to macroscopic models of viscous fingering for three-component, two-phase flows [11; 12] may eventually lead to the development of Riemann solvers that incorporate these effects.

The Riemann problem consists in solving a system of conservation laws in an infinite one-dimensional domain, with piecewise constant initial data separated by a single discontinuity. The development of analytical solutions to the Riemann problem of multiphase, multicomponent flow has received considerable attention over the past two decades (see, e.g. [3] and the references therein). Riemann solutions have been constructed for two-phase and three-phase systems with complex phase behavior for particular initial and injection conditions. However, the development of complete Riemann solvers is a much more challenging task. A Riemann solver is a mathematical algorithm that provides the solution to the Riemann problem for *any* initial and injection states. A Riemann solver for polymer flooding was originally presented by Isaacson [13], and then extended by Johansen and Winther to account for adsorption in two-component [14] and multicomponent systems [15; 16]. The principle behind polymer flooding is the addition of a *water-soluble* polymer to the injected water to *increase* its viscosity and, consequently, the efficiency of a waterflood. We are interested in miscible flooding, where the injected solvent readily

mixes with the *oil* in place, and *reduces* the viscosity of the hydrocarbon phase. However, under a proper change of variables, the mathematical structure of the equations is virtually identical to that of polymer flooding. Therefore, we rely heavily on the developments of Isaacson [13] and Johansen and Winther [14] when formulating the complete Riemann solver for first-contact miscible flooding. We extend the formulation (slightly) by accounting for the presence of connate water and residual oil. We also pay special attention to the efficient implementation of the analytical solver, because typical applications require the evaluation of hundreds of millions of Riemann problems [9].

An outline of the paper is as follows. In Section 2 we present the mathematical model describing the first-contact miscible system, and introduce the conservation variables employed in characterizing the solution. We comment on the mathematical character of the system of equations, highlighting the fact that it is not strictly hyperbolic. In Section 3 we describe the different waves that may be present, and the complete solution to the Riemann problem. In Section 4 we gather the main conclusions and anticipate the use of the analytical Riemann solver in the front-tracking/streamline framework described in detail in Part 2.

2 Mathematical model

2.1 Governing equations

We derive briefly the governing equations for one-dimensional, two-phase, three-component flow in porous media. The three components are referred to as water (w), oil (o) and solvent or gas (g). In what follows, we shall assume that water is immiscible, and forms an aqueous phase (w). We shall also assume that the two hydrocarbon components (oil and solvent) are fully miscible, and form a nonaqueous hydrocarbon phase (h).

The one-dimensional conservation equation for each of the components can be written as:

$$\frac{\partial m_i}{\partial t} + \frac{\partial F_i}{\partial x} = 0, \qquad i = w, o, g, \tag{1}$$

where m_i is the mass of component i per unit volume of porous medium, and F_i is the mass flux of that component. The mass densities are expressed in the following form:

$$m_w = \rho_w \phi S_w, \tag{2}$$

$$m_o = \rho_h \phi S_h \chi_o, \tag{3}$$

$$m_g = \rho_h \phi S_h \chi_g, \tag{4}$$

where ρ_α ($\alpha = w, h$) are the densities of each phase, ϕ is the porosity, S_α are the saturations (volume fractions of each phase), and χ_j ($j = o, g$) are the mass fractions of oil and solvent in the hydrocarbon phase. Equations (2)–(4) are subject to the following constraints:

$$S_w + S_h \equiv 1, \tag{5}$$

$$\chi_o + \chi_g \equiv 1. \tag{6}$$

The mass flux of each component, assuming that the macroscopic effects of viscous fingering are negligible, is given by:

$$F_w = \rho_w \phi v_w, \tag{7}$$

$$F_o = \chi_o \rho_h \phi v_h, \tag{8}$$

$$F_g = \chi_g \rho_h \phi v_h, \tag{9}$$

where v_α are the average velocities of each phase. A constitutive model for the phase velocities is given by the multiphase extension of Darcy's law. Neglecting the effect of gravity and capillary forces, they take the form:

$$v_w = -\frac{k}{\phi}\frac{k_{rw}}{\mu_w}\nabla p, \tag{10}$$

$$v_h = -\frac{k}{\phi}\frac{k_{rh}}{\mu_h}\nabla p, \tag{11}$$

where k is the absolute permeability of the medium, p is the pressure, and $k_{r\alpha}$ and μ_α are the relative permeability and dynamic viscosity of the α-phase, respectively. For the purpose of this paper, we shall assume that relative permeabilities are functions of the phase saturation only.

Using Equations (2)–(9) in Equation (1), and assuming incompressible fluids which do not experience volume change in mixing ($\rho_\alpha = \text{const}$) and rigid medium ($\phi = \text{const}$), the mass conservation equations for all three components are written as:

$$\frac{\partial S_w}{\partial t} + \frac{\partial v_w}{\partial x} = 0, \tag{12}$$

$$\frac{\partial((1-S_w)(1-\chi_g))}{\partial t} + \frac{\partial((1-\chi_g)v_h)}{\partial x} = 0, \tag{13}$$

$$\frac{\partial((1-S_w)\chi_g)}{\partial t} + \frac{\partial(\chi_g v_h)}{\partial x} = 0. \tag{14}$$

Summing Equations (12)–(14), we obtain the *pressure equation*:

$$\frac{\partial v_T}{\partial x} = 0, \tag{15}$$

where $v_T := v_w + v_h$ is the total velocity. The pressure equation is an elliptic equation, which dictates that the total velocity is at most a function of time. We introduce the fractional flow functions:

$$f_w := \frac{\lambda_w}{\lambda_T}, \tag{16}$$

$$f_h := \frac{\lambda_h}{\lambda_T}, \tag{17}$$

where $\lambda_\alpha = k_{r\alpha}/\mu_\alpha$ is the relative mobility of the α-phase, and $\lambda_T := \lambda_w + \lambda_h$ is the total mobility. With these definitions, a set of two independent conservation equations is:

$$\frac{\partial S_w}{\partial t} + v_T \frac{\partial f_w}{\partial x} = 0, \tag{18}$$

$$\frac{\partial((1-S_w)\chi_g)}{\partial t} + v_T \frac{\partial((1-f_w)\chi_g)}{\partial x} = 0. \tag{19}$$

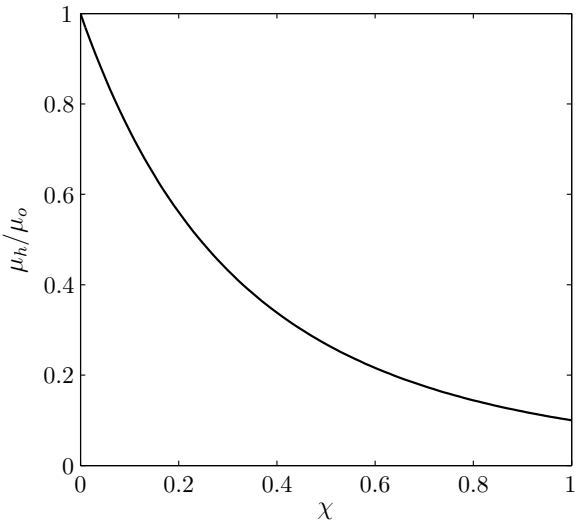

Figure 1. Typical dependence of the hydrocarbon viscosity on the solvent mass fraction.

It proves useful to express the governing equations above in terms of the following *conservation variables:*

$$S \equiv S_w \ : \quad \text{water saturation,} \tag{20}$$

$$C \equiv (1 - S_w)\chi_g \ : \quad \text{solvent concentration.} \tag{21}$$

In what follows, we drop the subscript from the solvent mass fraction, $\chi \equiv \chi_g$. After proper re-scaling of the time variable to eliminate the total velocity and letting f denote the water fractional flow function, the final form of the conservation equations is:

$$\frac{\partial S}{\partial t} + \frac{\partial f}{\partial x} = 0, \tag{22}$$

$$\frac{\partial C}{\partial t} + \frac{\partial}{\partial x}\left(\frac{1-f}{1-S}C\right) = 0. \tag{23}$$

To close the mathematical model, we must provide constitutive relations for the hydrocarbon viscosity and the relative permeabilities. The viscosity of the hydrocarbon phase depends on the viscosities of the oil and gas components μ_o and μ_g (taken as constants) and the gas mass fraction χ in the hydrocarbon phase. Since the gas viscosity is lower (usually much lower) than the oil viscosity, the hydrocarbon viscosity is a decreasing function of the gas mass fraction (see **Figure 1**).

We assume that the hydrocarbon relative permeability does not depend on the amount of solvent. In particular, this means that the residual hydrocarbon saturation is invariant. Thus, relative permeabilities of the aqueous and hydrocarbon phases are functions of the water saturation only. Typical behavior of these functions is shown in **Figure 2**, where we account for the presence of connate water and residual oil. As a result, the fractional flow is a function of both water saturation and solvent concentration:

$$f = \frac{\frac{k_{rw}(S)}{\mu_w}}{\frac{k_{rw}(S)}{\mu_w} + \frac{k_{rh}(S)}{\mu_h(\chi)}} = f(S, C). \tag{24}$$

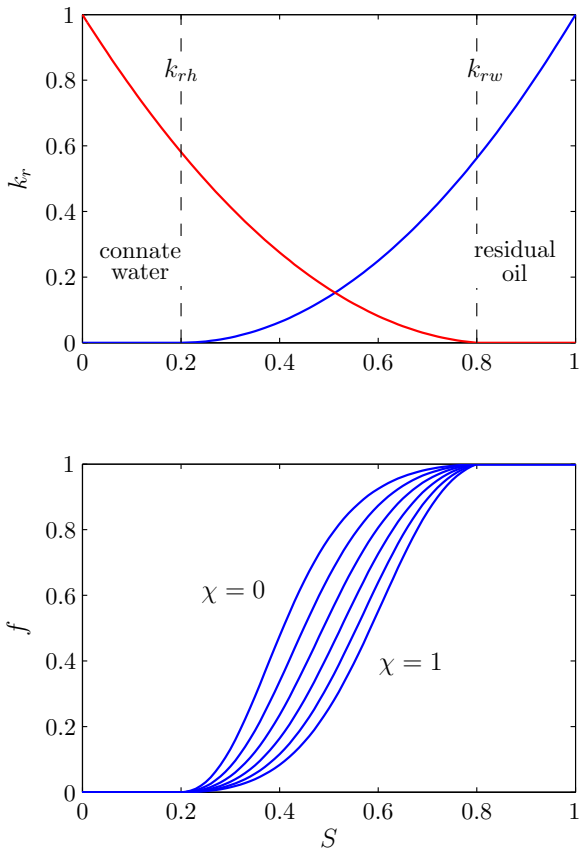

Figure 2. Top: relative permeabilities of the water and hydrocarbon phases. Bottom: dependence of the fractional flow function on the solvent mass fraction.

Since the hydrocarbon viscosity decreases with the solvent fraction, the overall mobility of the hydrocarbon phase is enhanced, resulting in lower values of the water fractional flow. The dependence of the fractional flow function on the solvent mass fraction is illustrated in **Figure 2**.

2.2 Mathematical character of the equations

We express the system of conservation laws (22)–(23) in vector form:

$$\partial_t \begin{bmatrix} S \\ C \end{bmatrix} + \partial_x \begin{bmatrix} f \\ \frac{1-f}{1-S} C \end{bmatrix} = \begin{bmatrix} 0 \\ 0 \end{bmatrix}. \tag{25}$$

The solution vector (S, C) is restricted to lie on the unit triangle:

$$\mathcal{U} \equiv \{(S, C) : S \geq 0,\ C \geq 0,\ S + C \leq 1\}. \tag{26}$$

For smooth solutions, the system (25) can be written as

$$\partial_t \begin{bmatrix} S \\ C \end{bmatrix} + A(S, C) \partial_x \begin{bmatrix} S \\ C \end{bmatrix} = \begin{bmatrix} 0 \\ 0 \end{bmatrix}, \tag{27}$$

where A is the Jacobian matrix of the system:

$$A(S,C) := \begin{bmatrix} \frac{\partial f}{\partial S} & \frac{\partial f}{\partial C} \\ \left(\frac{1-f}{1-S} - \frac{\partial f}{\partial S}\right)\frac{C}{1-S} & \frac{1-f}{1-S} - \frac{\partial f}{\partial C}\frac{C}{1-S} \end{bmatrix}. \tag{28}$$

The local character of the system is determined by the eigenvalues and eigenvectors of the Jacobian matrix [17]. The eigenvalues are given by:

$$\begin{aligned} \nu_s = \nu_s(S,C) &= \frac{\partial f}{\partial S} - \frac{\partial f}{\partial C}\frac{C}{1-S}, \\ \nu_c = \nu_c(S,C) &= \frac{1-f}{1-S}, \end{aligned} \tag{29}$$

and the corresponding eigenvectors are:

$$\begin{aligned} r_s &= \begin{bmatrix} 1 \\ -\frac{C}{1-S} \end{bmatrix}, \\ r_c &= \begin{bmatrix} \frac{\partial f}{\partial C} \\ \frac{1-f}{1-S} - \frac{\partial f}{\partial S} \end{bmatrix}. \end{aligned} \tag{30}$$

The eigenvalues ν_s and ν_c are the characteristic speeds of propagation of waves of the S- and C-family, respectively. The system is hyperbolic if the eigenvalues are real, and strictly hyperbolic if the eigenvalues are real and distinct. In the latter case, the matrix is diagonalizable and there exist two real and linearly independent eigenvectors. If the two eigenvalues are complex conjugates, the system is said to be elliptic.

It is easy to show that the system (25) is hyperbolic, but not everywhere strictly hyperbolic. Loss of strict hyperbolicity occurs in two regions of the composition triangle. First, in the region of residual oil, both eigenvalues are identically equal to zero. The Jacobian matrix is the zero matrix, and every direction is characteristic. Second, there is a curve in phase space at which the eigenvalues coincide, $\nu_s = \nu_c$. This curve divides the unit triangle $\mathcal{U}$ into two regions:

$$\begin{aligned} \mathcal{L} &\equiv \{(S,C) : \nu_s < \nu_c\}, \\ \mathcal{R} &\equiv \{(S,C) : \nu_s > \nu_c\}. \end{aligned} \tag{31}$$

We denote this curve as the *transition curve* $\mathcal{T}$ because the two families of eigenvalues change order as $\mathcal{T}$ is crossed. Since the fractional flow function is monotonic with respect to the solvent mass fraction χ, the transition curve intersects each line $\chi = \text{const}$ at exactly one point.

For the first-contact miscible model considered in this paper, the Jacobian matrix is not diagonalizable on $\mathcal{T}$, that is, A has only one independent eigenvector:

$$r_s\big|_{\mathcal{T}} = r_c\big|_{\mathcal{T}} = \begin{bmatrix} 1 \\ -\frac{C}{1-S} \end{bmatrix}. \tag{32}$$

The system is said to have a parabolic degeneracy on $\mathcal{T}$. This behavior is qualitatively very different from that of a model that assumes constant hydrocarbon viscosity. In such model, because the fractional flow f is a function of S only, the system is a multiple of the identity along the transition curve, and every direction is characteristic.

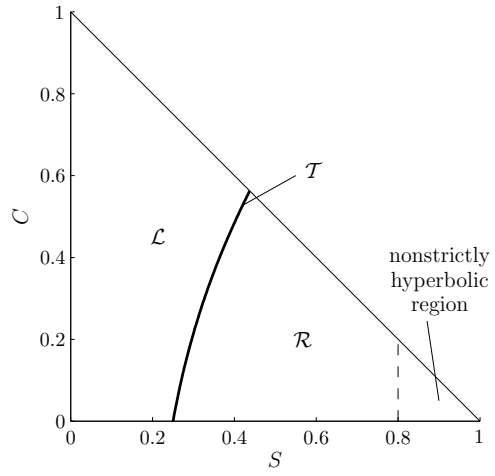

Figure 3. Transition curve $\mathcal{T}$ ($\nu_s = \nu_c$) and the regions $\mathcal{L}$ ($\nu_s < \nu_c$) and $\mathcal{R}$ ($\nu_s > \nu_c$) on the ternary diagram.

3 The Riemann problem

The Riemann problem consists in finding the weak solution to the system of hyperbolic conservation laws:

$$\partial_t u + \partial_x F = 0, \quad -\infty < x < \infty, \quad t > 0, \tag{33}$$

with the following initial conditions:

$$u(x,0) = \begin{cases} u_l & \text{if } x < 0, \\ u_r & \text{if } x \geq 0. \end{cases} \tag{34}$$

The state $u_l = (S_l, C_l)$ is the 'left' or 'injected' state, and $u_r = (S_r, C_r)$ is the 'right' or 'initial' state. The system of equations (33) and the initial condition (34) are invariant under uniform stretching of coordinates $(x,t) \mapsto (cx, ct)$. The solution must consist of centered waves emanating from the origin $(x,t) = (0,0)$. Therefore, we seek a self-similar solution

$$u(x,t) = U(\zeta), \tag{35}$$

where the similarity variable is $\zeta = x/t$.

3.1 Wave types

In this section we describe the types of centered waves that arise in the solution of the Riemann problem of miscible three-component flow.

3.1.1 Integral curves and Hugoniot locus

If the solution $U(\zeta)$ is smooth, it must satisfy

$$A(U)U' = \zeta U', \tag{36}$$

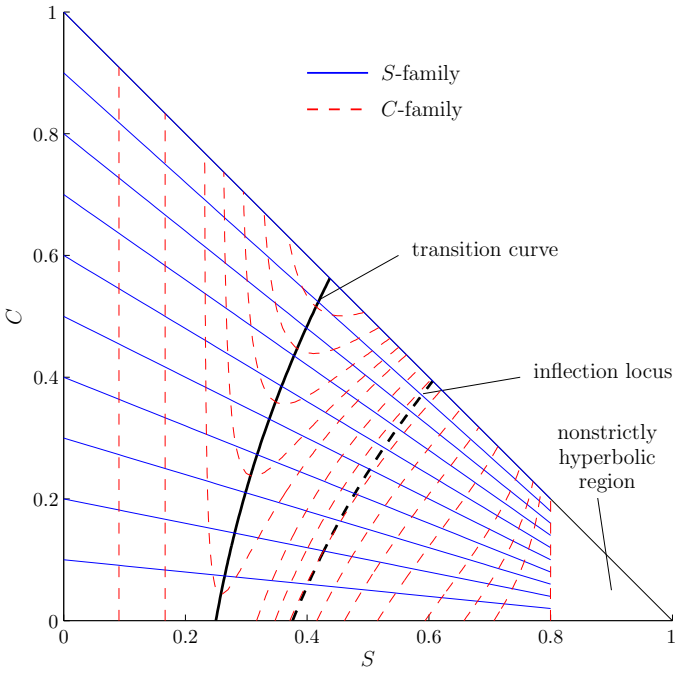

Figure 4. Integral curves of the S-family (solid line) and C-family (dashed line) on the ternary diagram. Also shown are the inflection locus of the S-family and the transition curve.

that is, ζ is an eigenvalue and U' is the corresponding eigenvector. Therefore, smooth waves (rarefactions) must lie on an integral curve of the right eigenvectors. States U along an integral curve are defined by the differential equation

$$\frac{\mathrm{d}U}{\mathrm{d}\tau} = r_i(U(\tau)), \quad i = s, c. \tag{37}$$

Performing the integration analytically, the two families of integral curves are given by the equations:

$$\begin{aligned} S\text{-family}: &\quad \frac{C}{1-S} = \text{const}, \\ C\text{-family}: &\quad \nu_c = \text{const}. \end{aligned} \tag{38}$$

The derivation of the equation for the S-family curves is obvious from the expression of the corresponding eigenvector r_s in Equation (30). The equation for the C-family can be obtained by noting that $\nabla\nu_c \cdot r_c \equiv 0$, that is the vector $\nabla\nu_c$ in phase space is everywhere perpendicular to the eigenvector r_c. Therefore, curves of the form $\nu_c = \text{const}$ must be integral curves of r_c. In the context of compositional displacements, integral curves of the S-family are known as *tie-line* paths, and curves of the C-family are termed *nontie-line paths* [3]. The integral curves of the system of interest are shown in **Figure 4**.

Discontinuous solutions must satisfy an integral version of the mass conservation equations, known as the Rankine–Hugoniot conditions. The set of states u that can be joined to a reference state u_r by a discontinuity satisfy:

$$F(u) - F(u_r) = \sigma\ (u - u_r), \tag{39}$$

where σ is the speed of propagation of the discontinuity. For the flux vector F of the first-contact miscible problem, Equation (39) admits two families of solutions, which define the Hugoniot locus of the S- and C-family. In general, integral curves and Hugoniot loci do not coincide, but they have second order tangency (same slope and curvature) at any given state, so they are locally very similar.

The integral curves of the miscible system have the following special features: (1) integral curves of the S-family are straight lines, which means that they have zero curvature; (2) the eigenvalue ν_c is constant along integral curves of the C-family, which means that these curves correspond to contact discontinuities. The immediate consequence of these properties is that, for the solvent system, Hugoniot loci and integral curves *coincide*.

3.1.2 Waves of the S-family (Tie-line waves)

Waves of the S-family are solutions of the classical Buckley–Leverett equation. The wave curves are straight lines on composition space, corresponding to lines of constant solvent mass fraction

$$\chi = \text{const.} \tag{40}$$

The characteristic velocity ν_s is not constant along integral curves of the S-family. Let us define

$$V_s(u) := \nabla \nu_s(u) \cdot r_s(u). \tag{41}$$

Since the convexity function V_s changes sign, the S-field is a nongenuinely nonlinear field in the sense of Lax [18]. The *inflection locus* is the set of states where $V_s = 0$, which separates regions of different convexity (see **Figure 4**). In our model, the fractional flow function is S-shaped, so the inflection locus intersects each tie-line at exactly one point, which corresponds to a *maximum* of the eigenvalue ν_s. It can be shown that, under these conditions, a S-wave can only be of three types: rarefaction, shock, and rarefaction-shock [19]. The admissibility of a S-wave is based on the e-Lax entropy condition (convex-hull construction) [20; 21]. A robust and efficient algorithm for the determination of the wave structure in the Buckley–Leverett problem is presented elsewhere [22].

3.1.3 Waves of the C-family (Nontie-line waves)

The characteristic speed ν_c is constant along wave curves of the C-family. The C-field is a linearly degenerate field in the sense of Lax [18], and the waves of this family are contact discontinuities. The immediate computational benefit of this property is that evaluation of nontie-line paths does not require numerical integration of an ordinary differential equation: the C-waves are completely determined by the algebraic relation

$$\nu_c = \text{const.} \tag{42}$$

Application of the e-Lax entropy condition [21] precludes the possibility that a C-wave joins constant states on opposite sides of the transition curve [13].

3.2 Admissible wave sequences

In general, the solution to the Riemann problem consists of a sequence of the centered waves described in the previous section. Before describing the complete solution, we give the admissible sequences of waves that may be present.

3.2.1 The case $u_l \xrightarrow{\mathcal{C}} u_m \xrightarrow{\mathcal{S}} u_r$

Adapting the analysis of Isaacson [13] to our model problem, it can be shown that the sequence of waves $u_l \xrightarrow{\mathcal{C}} u_m \xrightarrow{\mathcal{S}} u_r$, that is, the combination of a slower C-wave with a faster S-wave, is admissible only in the following three cases:

(a) If $u_m \in \mathcal{T}$ and $u_r \in \mathcal{R}$.

(b) If $u_m \in \mathcal{R}$ and $u_r \in \mathcal{R}$.

(c) If $u_m \in \mathcal{R}$ and $u_r \in \mathcal{L}$ such that $\nu_c(u_r) \geq \nu_c(u_m)$.

Examples of each of these wave sequences are given in **Figure 5**. The top row of figures show admissible sequences of wave curves in composition space. The bottom row of figures show the fractional flow curve corresponding to the tie-line passing through the intermediate state u_m. In all three cases, the characteristic speed of the C-wave (slope of the dashed line) is less than the characteristic speed of the S-wave (slope of the solid line), indicating admissibility of the wave sequence. In Case (a), u_m is *not* a true intermediate constant state, as the speed of both waves are equal at that point. Therefore, the sequence $\mathcal{CS}$ is in fact a single, coherent wave group.

3.2.2 The case $u_l \xrightarrow{\mathcal{S}} u_m \xrightarrow{\mathcal{C}} u_r$

Similarly, it can be shown that the sequence of waves $u_l \xrightarrow{\mathcal{S}} u_m \xrightarrow{\mathcal{C}} u_r$, that is, the combination of a slower S-wave with a faster C-wave, is admissible only in the following three cases:

(a) If $u_m \in \mathcal{T}$ and $u_l \in \mathcal{L}$.

(b) If $u_m \in \mathcal{L}$ and $u_l \in \mathcal{L}$.

(c) If $u_m \in \mathcal{L}$ and $u_l \in \mathcal{R}$ such that $\nu_c(u_l) \geq \nu_c(u_m)$.

In **Figure 6** we show examples of each of these wave pairs, illustrating the sequence of wave curves on the composition diagram and the fractional flow curve of the tie-line passing through u_m. Once again, Case (a) corresponds to a single, coherent wave group, in which the C-wave and the S-wave join with equal speeds, and the state u_m in *not* an intermediate constant state.

3.3 Solution of the Riemann problem

The global solution of the Riemann problem is obtained by joining waves that form a compatible sequence. Motivated by the admissible wave structure of Cases 1 and 2 above, and following Isaacson [13], we define several regions in the composition diagram that will allow a straightforward characterization of the wave structure of the solution.

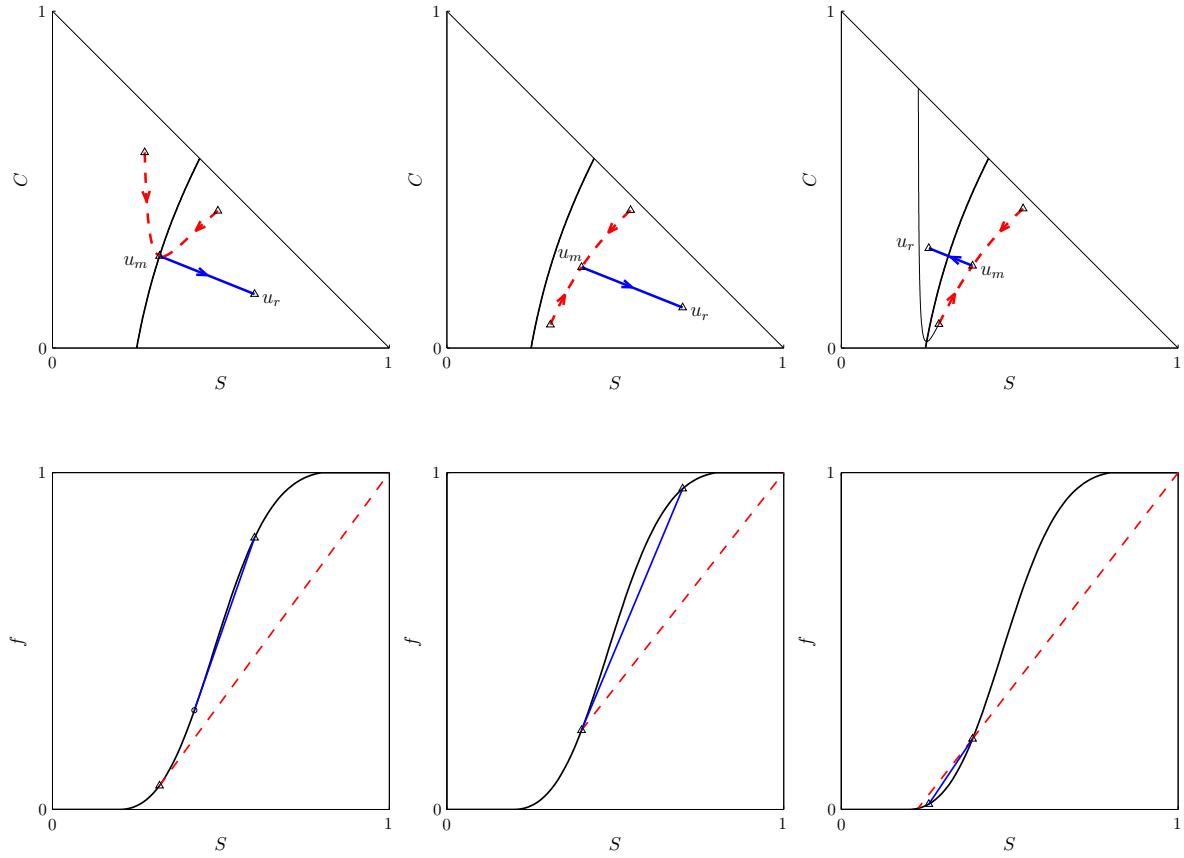

(a) $u_m \in \mathcal{T}$, $u_r \in \mathcal{R}$ (b) $u_m \in \mathcal{R}$, $u_r \in \mathcal{R}$ (c) $u_m \in \mathcal{R}$, $u_r \in \mathcal{L}$

Figure 5. All three types of compatible wave sequences of type $u_l \xrightarrow{\mathcal{C}} u_m \xrightarrow{\mathcal{S}} u_r$.

- The case $u_l \in \mathcal{L}$ (**Figure 7**(a)): One must first identify the tie-line $\chi = \chi(u_l)$ associated with the left state, and the intersection u_t of this tie-line and the transition curve $\mathcal{T}$. Then, we define the following three nonoverlapping regions that cover the entire ternary diagram $\mathcal{U}$:

  1. Region $\mathcal{L}_1$: It contains the set of states u satisfying $\nu_s(u) < \nu_c(u)$ and $\nu_c(u) < \nu_c(u_t)$. Therefore, it is bounded from the right by the transition curve $\mathcal{T}$ and the left branch of the nontie-line passing through the intersection point u_t.
  2. Region $\mathcal{L}_2$: It contains the set of states u satisfying that $\nu_s(u) > \nu_c(u_t)$ and $\chi(u) > \chi(u_t)$. It is bounded from the left by the left branch of the nontie-line passing through u_t and from below by the tie-line passing through u_t.
  3. Region $\mathcal{L}_3$: It contains the set of states u satisfying that $\nu_s(u) > \nu_c(u)$ and $\chi(u) < \chi(u_t)$. It is bounded from the left by the transition curve $\mathcal{T}$ and from above by the tie-line passing through u_t.

- The case $u_l \in \mathcal{R}$ (**Figure 7**(b)): We first find the nontie-line $\nu_c = \nu_c(u_l)$ associated with the left state, and the intersection u_t of this nontie-line and the transition curve $\mathcal{T}$. It is important to note that this intersection point may be outside the ternary diagram. In that

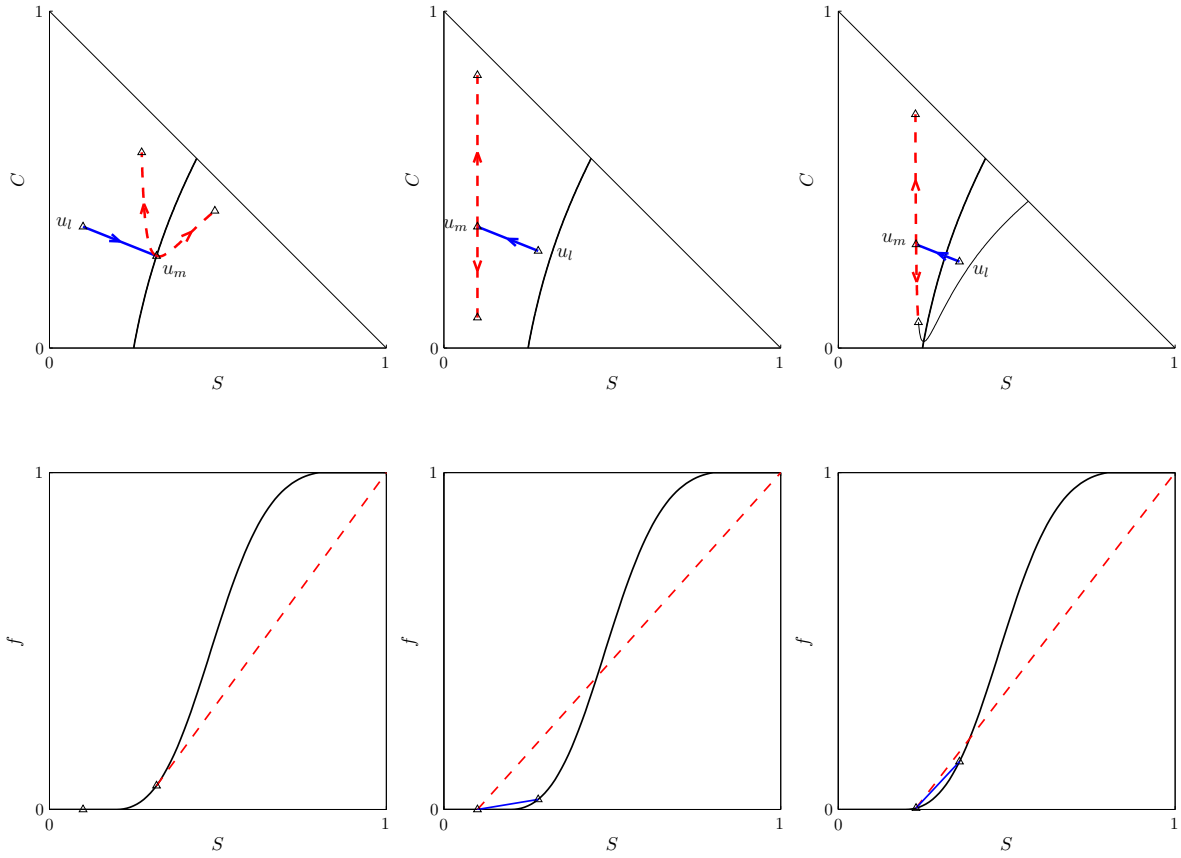

(a) $u_m \in \mathcal{T}$, $u_l \in \mathcal{L}$ (b) $u_m \in \mathcal{L}$, $u_l \in \mathcal{L}$ (c) $u_m \in \mathcal{L}$, $u_l \in \mathcal{R}$

Figure 6. All three types of compatible wave sequences of type $u_l \xrightarrow{\mathcal{S}} u_m \xrightarrow{\mathcal{C}} u_r$.

case, some of the regions defined below will be empty:

1. Region $\mathcal{R}_1$: It contains the set of states u satisfying that $\nu_s(u) < \nu_c(u)$ and $\nu_c(u) < \nu_c(u_t)$. If the intersection point u_t is inside the ternary diagram, this region is bounded from the right by the transition curve $\mathcal{T}$ and the left branch of the nontie-line passing through the intersection point u_t. Otherwise, it is bounded from the right entirely by the left branch of the nontie-line, and it is empty if $\nu_c(u_l) < 1$.
2. Region $\mathcal{R}_2$: It contains the set of states u satisfying that $\nu_s(u) > \nu_c(u_t)$ and $\chi(u) > \chi(u_t)$. If the intersection point u_t is inside the ternary diagram, this region is bounded from the left by the left branch of the nontie-line passing through u_t and from below by the tie-line passing through u_t. If u_t is outside the composition triangle, this region is only bounded from the left by the left branch of the nontie-line $\nu_c = \nu_c(u_l)$. If $\nu_c(u_l) < 1$, this region covers the entire triangle.
3. Region $\mathcal{R}_3$: It contains the set of states u satisfying that $\nu_s(u) > \nu_c(u)$ and $\chi(u) < \chi(u_t)$. If the intersection point u_t is inside the ternary diagram, this region is bounded from the left by the transition curve $\mathcal{T}$ and from above by the tie-line passing through u_t; otherwise it is empty.

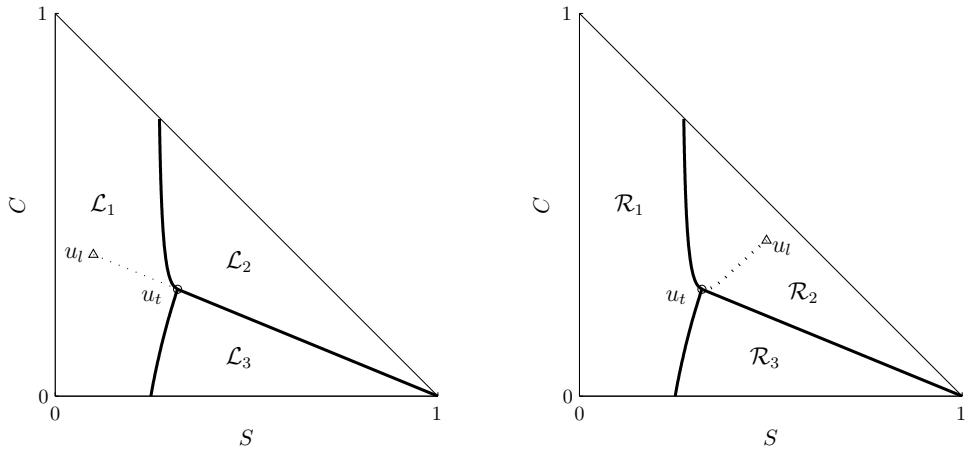

(a) $u_l \in \mathcal{L}$ (b) $u_l \in \mathcal{R}$

Figure 7. Regions on the ternary diagram defining the global wave structure of the Riemann solution.

We are now in position to give the global structure of the solution to the Riemann problem [13].

- The case $u_l \in \mathcal{L}$ (**Figure 8**): If the left state u_l belongs to the region $\mathcal{L}$, that is, if $\nu_s(u_l) < \nu_c(u_l)$, the global solution to the Riemann problem is of one of the following types:
  1. $u_r \in \mathcal{L}_1$ (**Figure 8**(a)): $u_l \xrightarrow{\mathcal{S}} u_m \xrightarrow{\mathcal{C}} u_r$.
  2. $u_r \in \mathcal{L}_2$ (**Figure 8**(b)): $u_l \xrightarrow{\mathcal{S}} u_t \xrightarrow{\mathcal{C}} u_m \xrightarrow{\mathcal{S}} u_r$.
  3. $u_r \in \mathcal{L}_3$ (**Figure 8**(c)): $u_l \xrightarrow{\mathcal{S}} u_m \xrightarrow{\mathcal{C}} u_t \xrightarrow{\mathcal{S}} u_r$.
- The case $u_l \in \mathcal{R}$ (**Figure 9**): If the left state u_l belongs to the region $\mathcal{R}$, that is, if $\nu_s(u_l) > \nu_c(u_l)$, the global solution to the Riemann problem is of one of the following types:
  1. $u_r \in \mathcal{R}_1$ (**Figure 9**(a)): $u_l \xrightarrow{\mathcal{S}} u_m \xrightarrow{\mathcal{C}} u_r$.
  2. $u_r \in \mathcal{R}_2$ (**Figure 9**(b)): $u_l \xrightarrow{\mathcal{C}} u_m \xrightarrow{\mathcal{S}} u_r$.
  3. $u_r \in \mathcal{R}_3$ (**Figure 9**(c)): $u_l \xrightarrow{\mathcal{S}} u_m \xrightarrow{\mathcal{C}} u_t \xrightarrow{\mathcal{S}} u_r$.

The solution to the Riemann problem presented above always exists (by construction) and is the unique solution satisfying the e-Lax entropy criteria [13; 18; 21]. It is important to note that all six solution types are of the form

$$u_l \xrightarrow{\mathcal{W}_1} u_m \xrightarrow{\mathcal{W}_2} u_r, \tag{43}$$

that is, two wave groups separated by an intermediate constant state. The slow wave $\mathcal{W}_1$ can be of type $\mathcal{S}$, $\mathcal{C}$ or $\mathcal{S}$-$\mathcal{C}$. The fast wave $\mathcal{W}_2$ can be of type $\mathcal{S}$, $\mathcal{C}$ or $\mathcal{C}$-$\mathcal{S}$. Of course, the solution may involve a single wave if the left and right states are on the same tie-line ($u_l \xrightarrow{\mathcal{S}} u_r$) or on the same nontie-line path ($u_l \xrightarrow{\mathcal{C}} u_r$).

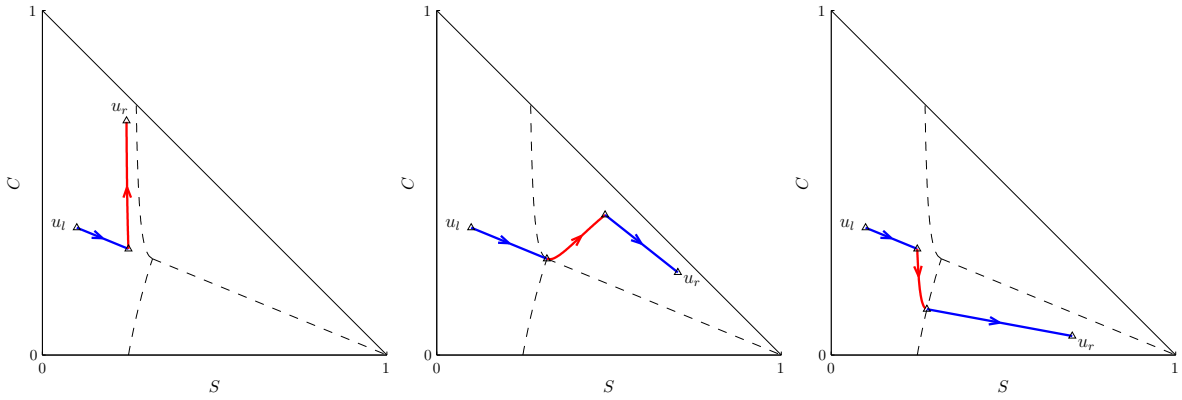

(a) $u_l \in \mathcal{L}$, $u_r \in \mathcal{L}_1$ (b) $u_l \in \mathcal{L}$, $u_r \in \mathcal{L}_2$ (c) $u_l \in \mathcal{L}$, $u_r \in \mathcal{L}_3$

Figure 8. Wave structure of the solution when $u_l \in \mathcal{L}$.

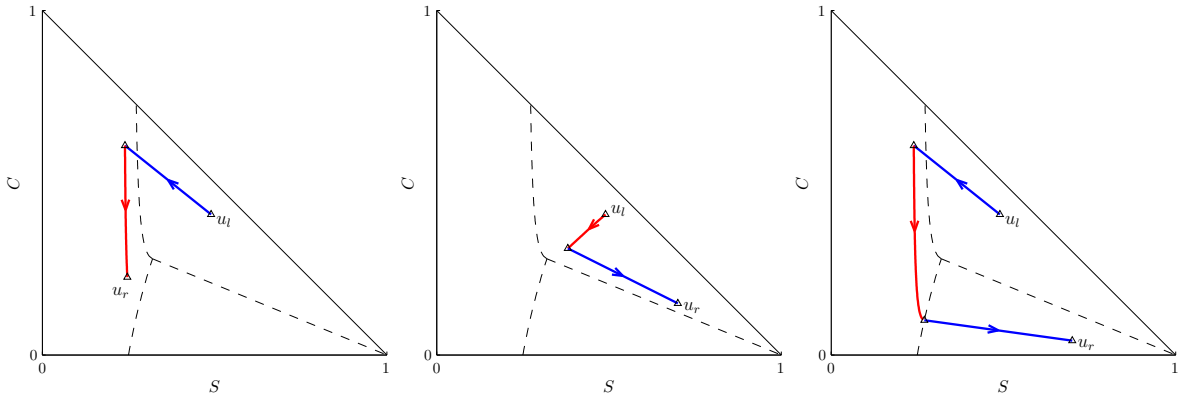

(a) $u_l \in \mathcal{R}$, $u_r \in \mathcal{R}_1$ (b) $u_l \in \mathcal{R}$, $u_r \in \mathcal{R}_2$ (c) $u_l \in \mathcal{R}$, $u_r \in \mathcal{R}_3$

Figure 9. Wave structure of the solution when $u_l \in \mathcal{R}$.

3.4 Convergence of finite difference solutions

The purpose of this section is to illustrate the difficulty of standard numerical methods in producing accurate solutions to the Riemann problem. The slow convergence of finite difference solutions to the analytical solution of nonstrictly hyperbolic conservation laws has been noted by many authors [14; 23; 24]. The main reason is the presence of contact discontinuities in the solution. Contact discontinuities are indifferent waves and, unlike genuine shocks, are *not* self-sharpening. As a result, some essential features of the solution may be overwhelmed by numerical diffusion introduced by standard finite difference schemes. Other high-order finite difference methods (such as Essentially Non-oscillatory schemes [25]) will generally reproduce contact discontinuities much more accurately, but these methods are not commonly used in reservoir simulation.

In **Figure 10** we compare the analytical solution to a Riemann problem of type $\mathcal{R}_3$ with finite difference solutions on increasingly refined grids. We used the single-point upstream finite difference method, and a Crank-Nicolson scheme for integration in time. The time step was chosen so that the Courant number $Co = \sigma_{\max}\delta t/\delta x$ was approximately equal to 2. Results of the finite difference calculations are shown at time $t = 0.25$.

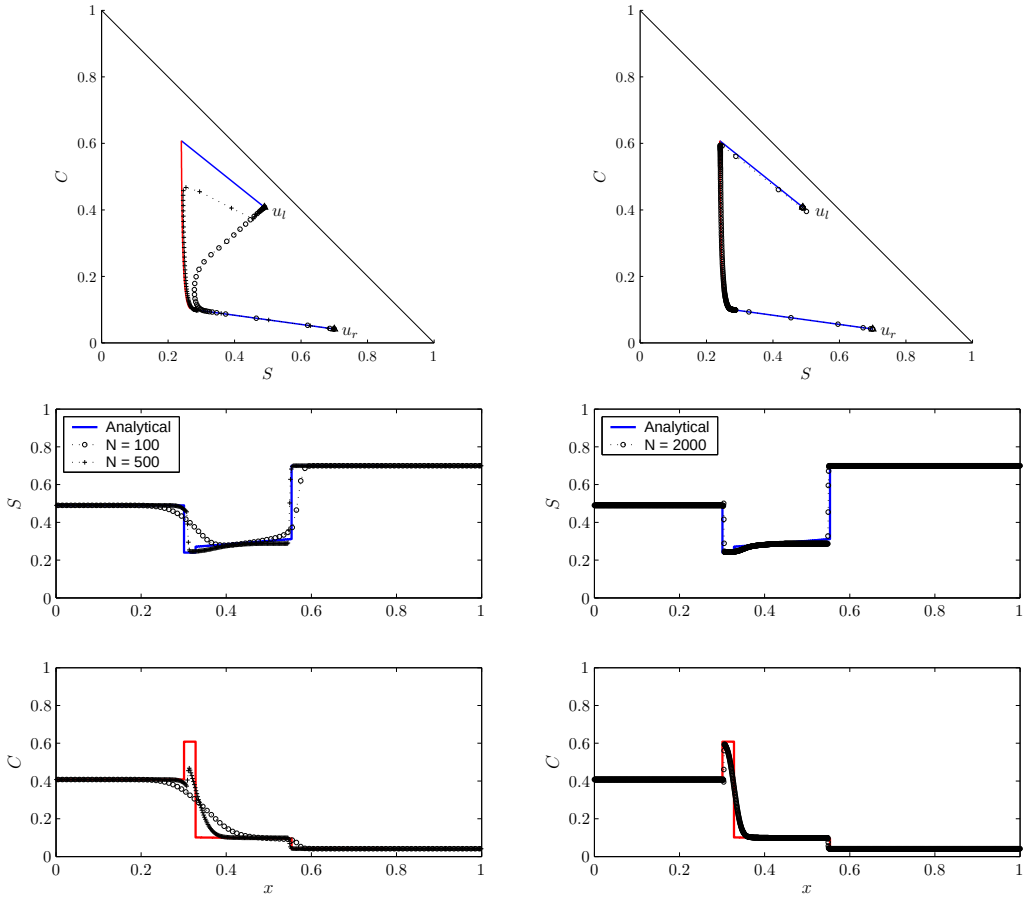

Figure 10. Comparison between analytical and finite difference solutions for a Riemann problem of type $\mathcal{R}_3$. Left: Numerical solution with 100 and 500 gridblocks. Right: Numerical solution with 2000 gridblocks.

One of the distinctive features of the solution is the presence of a contact discontinuity (transitional wave) of large amplitude, related to the formation of a solvent bank. It is apparent from the figure that the finite difference solutions with 100 and 500 gridblocks are unable to resolve this feature. In this case, an accurate solution requires a grid with at least 2000 cells.

4 Conclusions

In this paper we have described a mathematical model and the associated Riemann solver for the simulation of first-contact miscible gas injection processes. Under certain simplifying assumptions, the system describing two-phase, three-component, first-contact miscible flow is a 2×2 hyperbolic system. It is not, however, strictly hyperbolic. Using an analogy with the system of equations governing polymer flooding [13; 14], we give the complete solution to the Riemann problem. We show that the solution may involve more than two waves, one of which is always a contact discontinuity.

The efficiency of the front-tracking algorithm to be presented in Part 2 relies heavily on the availability of an analytical Riemann solver. The solvent system studied here has two features

that make the front-tracking scheme particularly attractive: (1) rarefaction curves and shock curves coincide in composition space, so there is no need to perform (an expensive) numerical integration to characterize rarefaction waves; (2) some waves are contact discontinuities, which are not self-sharpening. As shown in Section 3.4, such waves are very sensitive to numerical diffusion introduced by classical finite difference schemes, but they are resolved *exactly* in a front-tracking solution.

From the point of view of the physical model, the work presented here can be extended in a number of ways. An important extension is to account for viscous fingering. Two of the most commonly used macroscopic models for single-phase miscible displacements are those proposed by Koval [26] and Todd and Longstaff [27]. Blunt and coworkers proposed an extension of these models to two-phase, three-component, first-contact miscible flows [28; 29]. Analytical solutions to this model have been developed by Blunt and Christie [28] and, recently, in [11; 12]. These new solutions may eventually lead to the development of a full Riemann solver for multiphase first-contact miscible flow models that account for the macroscopic effect of viscous fingering. Another interesting but challenging extension would be to consider multicontact miscible problems, in which the hydrocarbon components do *not* mix in all proportions. Analytical solutions for particular initial and injection states have been presented recently by LaForce and Johns [30].

The use of the analytical Riemann solver in the context of front-tracking/streamline simulation is the subject of the second paper in this series [31].

Acknowledgements

R.J. gratefully acknowledges financial support from the industrial affiliates of the Stanford University Petroleum Research Institute for Numerical Simulation (SUPRI-B) and Gas Injection (SUPRI-C). K.-A.L. gratefully acknowledges financial support from the Research Council of Norway under grant number 158908/I30.

References

[1] F. I. Stalkup Jr. *Miscible Displacement*, volume 8 of *SPE Monograph Series*. Society of Petroleum Engineers, Dallas, TX, 1983.

[2] L. W. Lake. *Enhanced Oil Recovery*. Prentice-Hall, Englewood Cliffs, NJ, 1989.

[3] F. M. Orr Jr. *Theory of Gas Injection Processes*. Stanford University, 2005.

[4] G. A. Pope. The application of fractional flow theory to enhanced oil recovery. *Soc. Pet. Eng. J.*, 20(3):191–205, June 1980. *Petrol. Trans.* AIME, 269.

[5] F. G. Helfferich. Theory of multicomponent, multiphase displacement in porous media. *Soc. Pet. Eng. J.*, 21(1):51–62, February 1981. *Petrol. Trans.* AIME, 271.

[6] G. J. Hirasaki. Application of the theory of multicomponent, multiphase displacement to three-component, two-phase surfactant flooding. *Soc. Pet. Eng. J.*, 21(2):191–204, April 1981. *Petrol. Trans.* AIME, 271.

[7] Y. Wang and F. M. Orr Jr. Analytical calculation of the minimum miscibility pressure. *Fluid Phase Equilib.*, 139:101–124, 1997.

[8] K. Jessen, M. L. Michelsen, and E. H. Stenby. Global approach for calculation of the minimum miscibility pressure. *Fluid Phase Equilib.*, 153:251–263, 1998.

[9] K.-A. Lie and R. Juanes. A front-tracking method for the simulation of three-phase flow in porous media. *Comput. Geosci.*, 9(1):29–59, 2005.

[10] R. Juanes, K.-A. Lie, and V. Kippe. A front-tracking method for hyperbolic three-phase models. In *European Conference on the Mathematics of Oil Recovery, ECMOR IX*, volume 2, paper B025, Cannes, France, August 30–September 2 2004.

[11] R. Juanes and M. J. Blunt. Analytical solutions to multiphase first-contact miscible models with viscous fingering. *Transp. Porous Media*, 2005. (Accepted).

[12] R. Juanes, H. S. Al-Shuraiqi, A. H. Muggeridge, C. A. Grattoni, and M. J. Blunt. Experimental and numerical validation of an analytical model of viscous fingering in two-phase, three-component flow. *J. Fluid Mech.*, 2005. (Submitted).

[13] E. L. Isaacson. Global solution of a Riemann problem for a non-strictly hyperbolic system of conservation laws arising in enhanced oil recovery. Technical report, The Rockefeller University, New York, 1980.

[14] T. Johansen and R. Winther. The solution of the Riemann problem for a hyperbolic system of conservation laws modeling polymer flooding. *SIAM J. Math. Anal.*, 19(3):541–566, 1988.

[15] T. Johansen and R. Winther. The Riemann problem for multicomponent polymer flooding. *SIAM J. Math. Anal.*, 20(4):908–929, 1989.

[16] T. Johansen, A. Tveito, and R. Winther. A Riemann solver for a two-phase multicomponent process. *SIAM J. Sci. Comput.*, 10(5):846–879, 1989.

[17] E. Zauderer. *Partial Differential Equations of Applied Mathematics*. Series in Pure and Applied Mathematics. John Wiley & Sons, New York, 1983.

[18] P. D. Lax. Hyperbolic systems of conservation laws, II. *Comm. Pure Appl. Math.*, 10:537–566, 1957.

[19] F. Ancona and A. Marson. A note on the Riemann problem for general $n \times n$ conservation laws. *J. Math. Anal. Appl.*, 260:279–293, 2001.

[20] O. A. Oleinik. Discontinuous solutions of nonlinear differential equations. *Usp. Mat. Nauk. (N.S.)*, 12:3–73, 1957. English transl. in *Amer. Math. Soc. Transl. Ser.* 2, 26:95–172.

[21] T.-P. Liu. The Riemann problem for general 2×2 conservation laws. *Trans.* Amer. Math. Soc., 199:89–112, 1974.

[22] R. Juanes. Determination of the wave structure of the three-phase flow Riemann problem. *Transp. Porous Media*, 60(2):135–139, 2005.

[23] N. H. Risebro and A. Tveito. Front tracking applied to a nonstrictly hyperbolic system of conservation laws. *SIAM J. Sci. Stat. Comput.*, 12(6):1401–1419, 1991.

[24] K. Jessen, E. H. Stenby, and F. M. Orr. Interplay of phase behavior and numerical dispersion in finite-difference compositional simulation. *Soc. Pet. Eng. J.*, 9(2):193–201, June 2004.

[25] A. Harten, B. Engquist, S. Osher, and S. Chakravarthy. Uniformly high-order accurate essentially nonoscillatory schemes, III. *J. Comput. Phys.*, 71:231–241, 1987.

[26] E. J. Koval. A method for predicting the performance of unstable miscible displacements in heterogeneous media. *Soc. Pet. Eng. J.*, pages 145–150, June 1963. *Petrol. Trans.* AIME, 219.

[27] M. R. Todd and W. J. Longstaff. The development, testing and application of a numerical simulator for predicting miscible flood performance. *J. Pet. Technol.*, pages 874–882, July 1972.

[28] M. Blunt and M. Christie. How to predict viscous fingering in three component flow. *Transp. Porous Media*, 12:207–236, 1993.

[29] M. Blunt and M. Christie. Theory of viscous fingering in two phase, three component flow. *SPE Advanced Technology Series*, 2(2):52–60, 1994.

[30] T. LaForce and R. T. Johns. Composition routes for three-phase partially miscible flow in ternary systems. *Soc. Pet. Eng. J.*, 10(2):161–174, June 2005.

[31] R. Juanes and K.-A. Lie. Numerical modeling of multiphase first-contact miscible flows. Part 2. Front-tracking/streamline simulation. *Transp. Porous Media*, 2005. (Submitted).